Supplementary information for

A Stretchable, Conformable, Biocompatible Graphene Strain Sensor Based on Structured Hydrogel for Clinical Application

Yuting Cai [a, b,1], Jinbao Qin [c,1], Weimin Li[c], Abhishek Tyagi[b], Zhenjing Liu[b], Md Delowar Hossain[b], Haomin Chen[e], Hongwei Liu[b], Minghao Zhuang[b], Jiawen You[b], Feng Xu[d], Xinwu Lu[c*], Dazhi Sun[a*], Zhengtang Luo[b*]

[a] *Department of Materials Science and Engineering, Southern University of Science and Technology, Shenzhen, Guangdong 518055, China*
[b] *Department of Chemical and Biological Engineering, and William Mong Institute of Nano Science and Technology, The Hong Kong University of Science and Technology, Clear Water Bay, Kowloon, Hong Kong*
[c] *Department of Vascular Surgery, Shanghai Ninth People's Hospital, Shanghai JiaoTong University, School of Medicine, Shanghai 200011, P. R. China*
[d] *Department of Mechanical and Aerospace Engineering, The Hong Kong University of Science and Technology, Clear Water Bay, Kowloon, Hong Kong*
[e] *Bioinspired Engineering and Biomechanics Center, Xi'an Jiaotong University, Xi'an, 710049, ShaanXi, P. R. China*
[f] *The Key Laboratory of Biomedical Information Engineering of Ministry of Education, School of Life Science and Technology, Xi'an Jiaotong University, Xi'an 710049, P.R. China*

*E-mail: keztluo@ust.hk, sundz@sustech.edu.cn, or luxinwu@shsmu.edu.cn
[1]These authors contributed equally to this work.

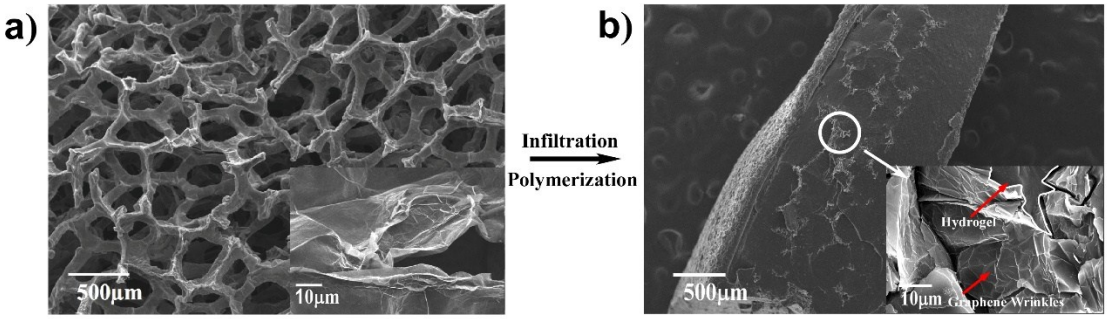

Figure S1. Morphology of GF and after encapsulation. (a) SEM micrographs of GF, the inset shows an enlarged view of GF matrix surface. **(b)** SEM micrographs of GF/PAM/CA strain sensor, the smooth part represents pure hydrogel while the inset shows an enlarged view of composites.

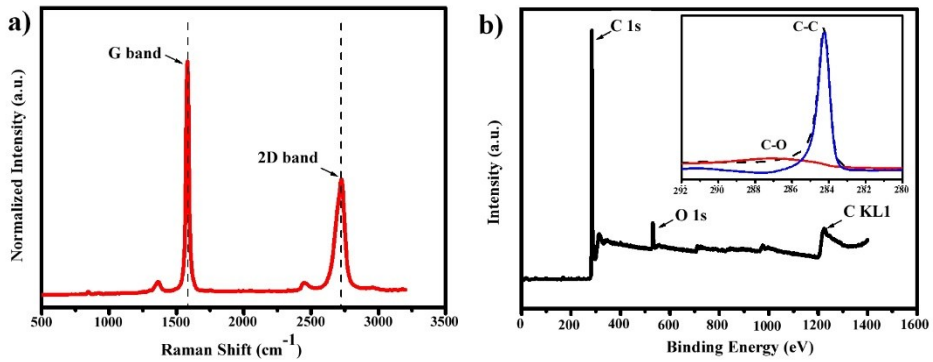

Figure S2. Characterization of 3D GF. (a) Typical Raman spectrum of GF. **(b)** XPS spectra of GF, the inset shows high-resolution C (1s) XPS spectra.

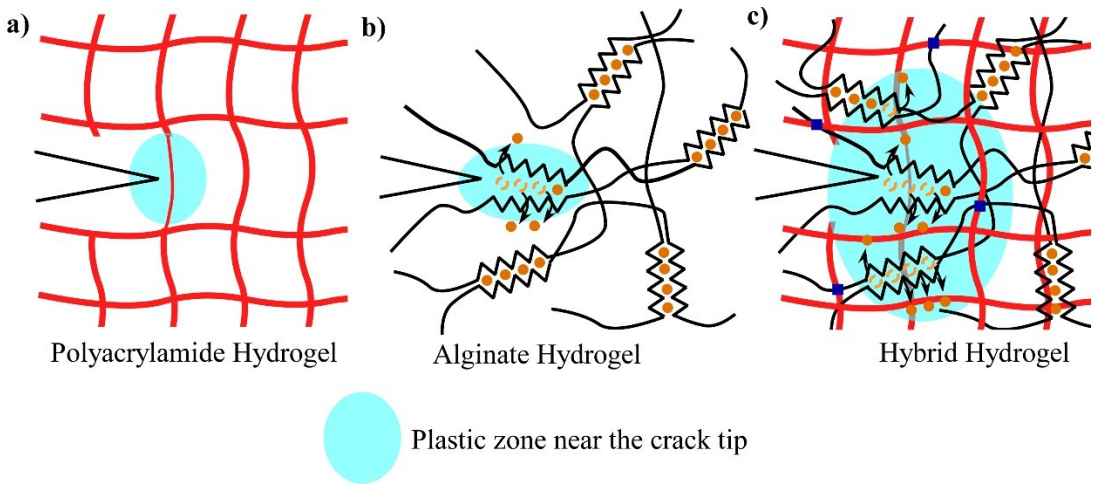

Figure S3. Synergy between alginate and polyacrylamide. (a) In the polyacrylamide gel, once a running crack appear, only the polyacrylamide chains crossing the crack plane need to break, and chains elsewhere remain intact. **(b)** In the alginate gel, once a running crack appear, only the ionic bonds crossing the crack need to break, and ionic crosslinks elsewhere remain intact. **(c)** In the hybrid gel, the polyacrylamide chains stabilize deformation and the ionic crosslinks between alginate chains break, double network transfer the load over a large zone and effectively dissipate energy.

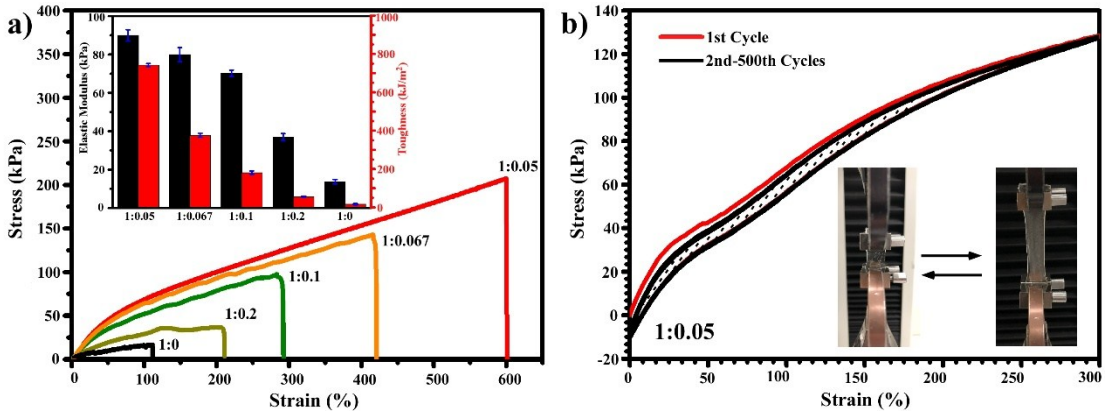

Figure S4. Mechanical properties of hydrogels. (a) Tensile stress–strain curves of hybrid hydrogel with different AM at a fixed concentration of CA. The ratio represents concentration of AM to concentration of CA.

The inset shows the toughness and elastic modulus are calculated from stress–strain curves of different hydrogels **(b)** Relaxation cycles for the 1:0.05 hydrogel with 500 cycles under a tension of 300%. The shaded area represents the area between the loading and unloading curves. The inset shows photographs of an PAM/CA hydrogel during the tensile test.

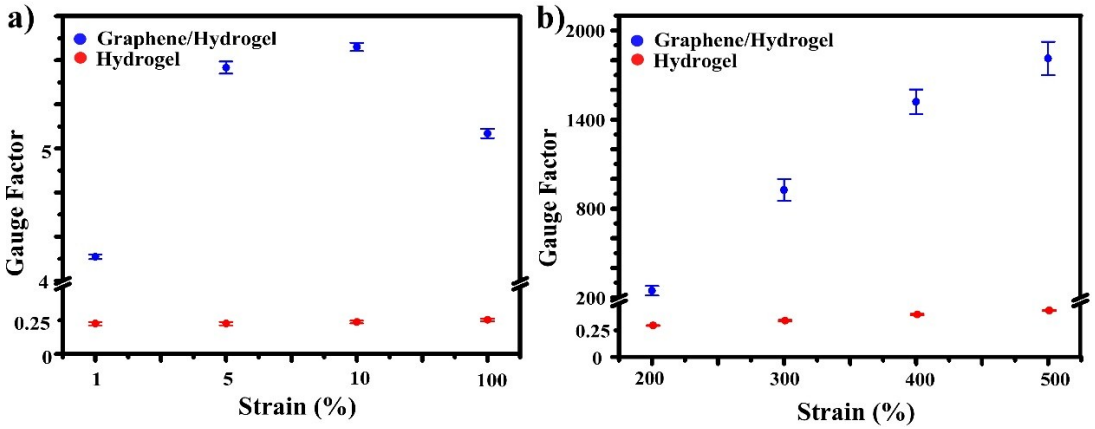

Figure S5. Sensing performance of GF/PAM/CA strain sensor at different strain. the gauge factor at 1% ,5%, 10%, 100%, 200%, 300%, 400%, 500% strain with error bar shows standard deviation (n = 3).

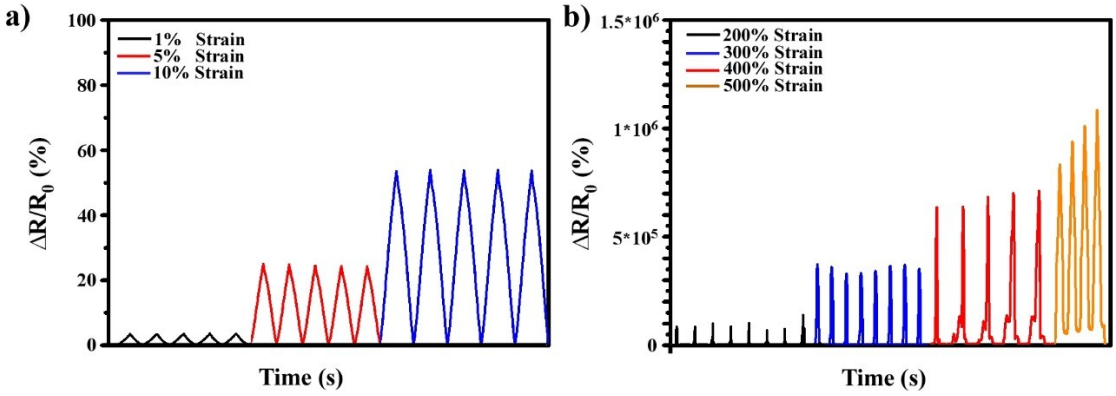

Figure S6. Sensing performance at different strain. Relative resistance change ($\Delta R/R_0$) of GF/PAM/CA composite at small **(a)** and large **(b)** strain. Error bar shows standard deviation (n = 3).

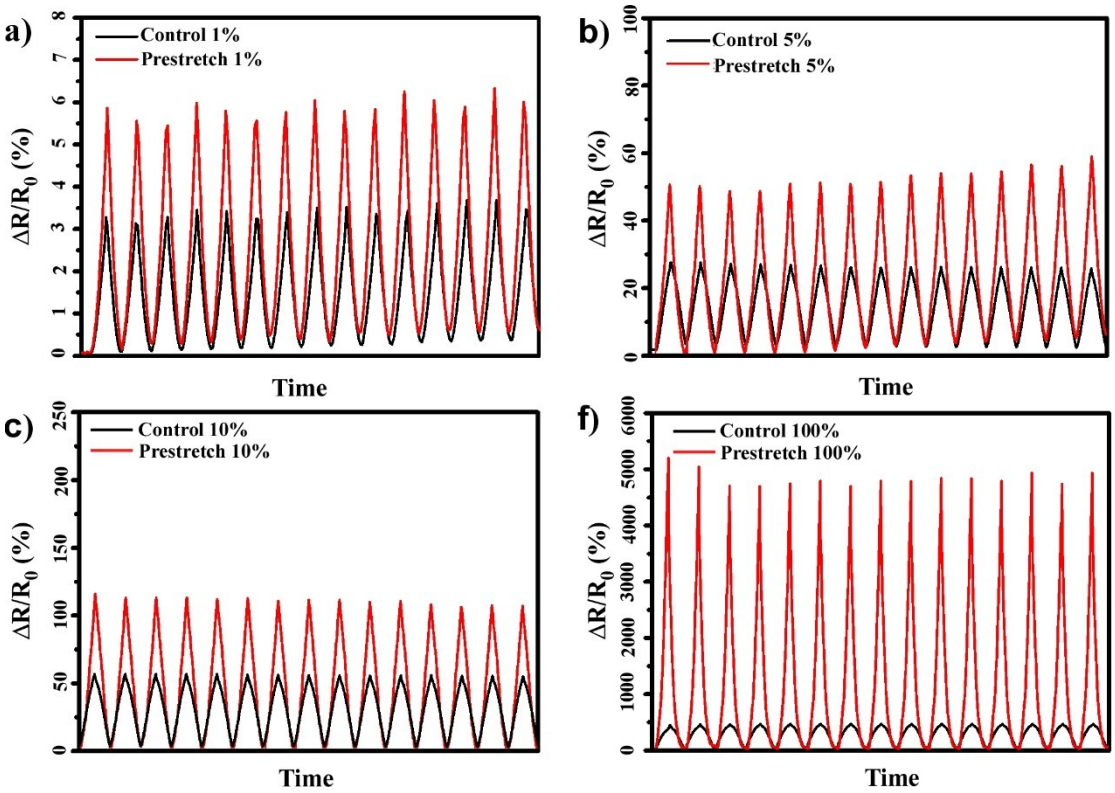

Figure S7. Sensing performance improvement after prestretch process. Relative resistance change ($\Delta R/R_0$) of GF/PAM/CA composite before (control group) and after large stretch (500% strain).

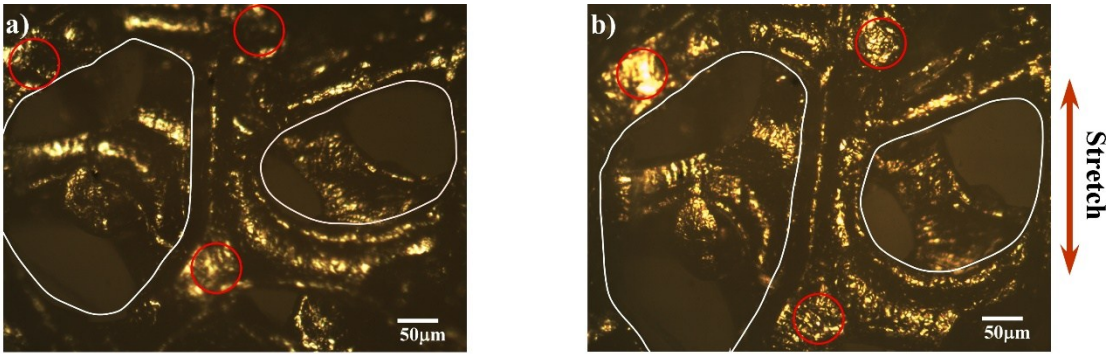

Figure S8. In-situ optical images of GF/PAM/CA strain sensor. (a) The initial status. **(b)** Under small strain (20%). Two white circles focus on two pores within the GF matrix**.** The y axis length of these two pores as illustrated by the white circles is increased under stretching, keeping the same deformation direction and ratio with strain. The growing shining spots denoted by red circles on GF matrix indicate that cracks initiate and propagate because cracks can reflect more light.

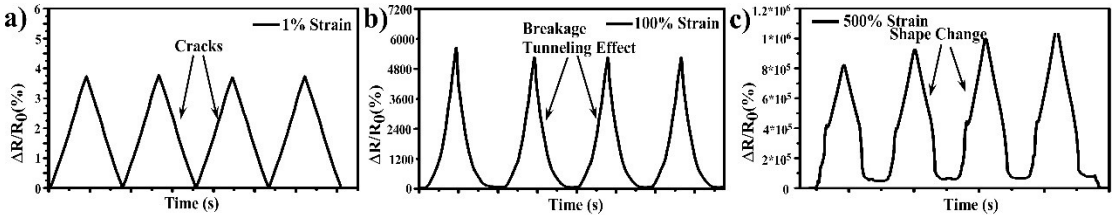

Figure S9. Change of relative resistance at different strain showing different patterns and mechanism. Carks generation step at small strain. Tunneling effect at middle strain. Geometrical effect at extremely large strain.

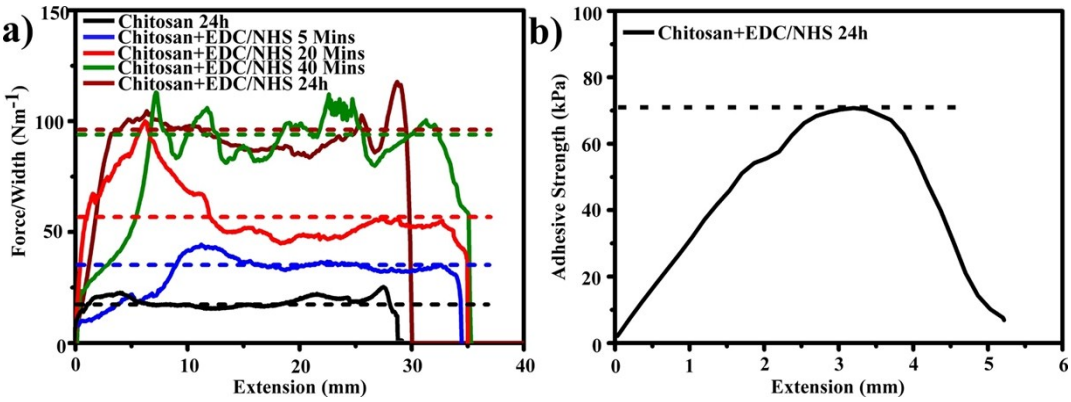

Figure S10. Adhesive performance of chitosan. (a) Force -extension curves of peeling tests after different reaction time. The adhesion energy is calculated based on the average value of force/width at the plateau region. The porcine skin is washed by water before adhesion. **(b)** Adhesion strength of chitosan bridge. For commercial fibrin glue the value is around 12kPa.

Figure S11. Detachment from the skin. Sensor can be removed by extra force with no residual hydrogel left on skin.

Table S1. Compositions of the prepared hydrogels

	SA (g)	AM (g)	$CaCl_2$ (g)	APS (g)	MBAA (g)	PBS solution (mL)
A	**0.2**	**4**	**0.016**	**0.04**	**0.02**	**10**
B	**0.2**	**3**	**0.016**	**0.03**	**0.015**	**10**
C	**0.2**	**2**	**0.016**	**0.02**	**0.01**	**10**
D	**0.2**	**1**	**0.016**	**0.01**	**0.005**	**10**
E	**0**	**1**	**0**	**0.01**	**0.005**	**10**

Considering high concentrations of CA can become too viscous which hinders the infiltration process and the poor water solubility of SA and pronounced hysteresis of pure CA hydrogel, only the concentration of AM are varied for this investigation. Besides, hydrogel made by high concentration AM is too rigid to damage GF network.